

# Optical properties of a bio-inspired gradient refractive index polymer lens

G. Beadie,<sup>1,\*</sup> James S. Shirk,<sup>1</sup> A. Rosenberg,<sup>1</sup> Paul A. Lane,<sup>1</sup> E. Fleet,<sup>1</sup> A. R. Kamdar,<sup>2</sup> Y. Jin,<sup>2</sup> M. Ponting,<sup>2</sup> T. Kazmierczak,<sup>2</sup> Y. Yang,<sup>2</sup> A. Hiltner,<sup>2</sup> and E. Baer<sup>2</sup>

<sup>1</sup>Optical Sciences Division, Naval Research Lab, 4555 Overlook Ave., SW, Washington, D.C. 20375, USA

<sup>2</sup>Department of Macromolecular Science and Center for Applied Polymer Research, Case Western Reserve University, 2100 Adelbert Road, Kent Hale Smith Bldg., Cleveland, OH, 44106, USA

\*Corresponding author: [guy.beadie@nrl.navy.mil](mailto:guy.beadie@nrl.navy.mil)

**Abstract:** The design, fabrication, and properties of one of a new class of gradient-index lenses are reported. The lens is an  $f/2.25$  GRIN singlet based on a nanolayered polymer composite material, designed to correct for spherical aberration. The light gathering and focusing properties of the polymer lens are compared to a homogeneous BK7 glass singlet with a similar f-number. The modulation transfer function of the polymer GRIN lens exceeded that of the homogeneous glass lens at all spatial frequencies and was as much as 3 times better at 5 cyc/mm. The weight of the polymer lens was approximately an order of magnitude less than the homogeneous glass lens.

©2008 Optical Society of America

OCIS codes: (110.2760) Gradient-index lenses; (160.5470) Polymers; (230.4170) Multilayers.

---

## References and links

1. D. A. Atchison, and G. Smith, "Continuous Gradient-Index and Shell Models of the Human Lens," *Vision Res.* **35**, 2529-2538 (1995).
2. L. F. Garner, G. Smith, S. Yao, and R. C. Augusteyn, "Gradient refractive index of the crystalline lens of the Black Oreo Dory (*Alloctytus Niger*): comparison of magnetic resonance imaging (MRI) and laser ray-trace methods," *Vision Res.* **41**, 973-979 (2001).
3. H. von Helmholtz, A. Gullstrand, J. von Kries, and W. Nagel, *Helmholtz's Treatise on Physiological Optics* (The Optical Society of America, Rochester, N.Y., 1924).
4. B. A. Moffat, D. A. Atchison, and J. M. Pope, "Age-related changes in refractive index distribution and power of the human lens as measured by magnetic resonance micro-imaging in vitro," *Vision Res.* **42**, 1683-1693 (2002).
5. L. Bergmann, C. Schaefer, and H. Niedrig, *Optics of Waves and Particles* (W. de Gruyter, Berlin; New York, 1999).
6. G. L. Walls, *The Vertebrate Eye and its Adaptive Radiation* (Hafner Pub. Co., New York, 1963).
7. W. S. Jagger, and P. J. Sands, "A wide-angle gradient index optical model of the crystalline lens and eye of the rainbow trout," *Vision Res.* **36**, 2623-2639 (1996).
8. Y. Jin, H. Tai, A. Hiltner, E. Baer, and J. S. Shirk, "New class of bioinspired lenses with a gradient refractive index," *J. Appl. Polym. Sci.* **103**, 1834-1841 (2007).
9. C. D. Mueller, S. Nazarenko, T. Ebeling, T. L. Schuman, A. Hiltner, and E. Baer, "Novel structures by microlayer coextrusion - Talc-filled PP, PC/SAN, and HDPE/LLDPE," *Polym. Eng. Sci.* **37**, 355-362 (1997).
10. J. Kerns, A. Hsieh, A. Hiltner, and E. Baer, "Comparison of irreversible deformation and yielding in microlayers of polycarbonate with poly(methylmethacrylate) and poly(styrene-co-acrylonitrile)," *J. Appl. Polym. Sci.* **77**, 1545-1557 (2000).
11. C. Mueller, V. Topolkaev, D. Soerens, A. Hiltner, and E. Baer, "Breathable polymer films produced by the microlayer coextrusion process," *J. Appl. Polym. Sci.* **78**, 816-828 (2000).
12. J. A. Reynolds, and J. M. Hough, "Formulae for Dielectric Constant of Mixtures," *Proc. Phys. Soc. London B* **70**, 769-775 (1957).
13. S. D. Fantone, "Optical Design with Spherical Index Gradients," *Appl. Opt.* **22**, 1815-1819 (1983).
14. J. M. Gordon, "Spherical gradient-index lenses as perfect imaging and maximum power transfer devices," *Appl. Opt.* **39**, 3825-3832 (2000).
15. Y. Koike, A. Kanemitsu, Y. Shioda, E. Nihei, and Y. Ohtsuka, "Spherical Gradient-Index Polymer Lens with Low Spherical-Aberration," *Appl. Opt.* **33**, 3394-3400 (1994).

# Report Documentation Page

Form Approved  
OMB No. 0704-0188

Public reporting burden for the collection of information is estimated to average 1 hour per response, including the time for reviewing instructions, searching existing data sources, gathering and maintaining the data needed, and completing and reviewing the collection of information. Send comments regarding this burden estimate or any other aspect of this collection of information, including suggestions for reducing this burden, to Washington Headquarters Services, Directorate for Information Operations and Reports, 1215 Jefferson Davis Highway, Suite 1204, Arlington VA 22202-4302. Respondents should be aware that notwithstanding any other provision of law, no person shall be subject to a penalty for failing to comply with a collection of information if it does not display a currently valid OMB control number.

1. REPORT DATE <b>27 JUN 2008</b>		2. REPORT TYPE		3. DATES COVERED <b>00-00-2008 to 00-00-2008</b>	
4. TITLE AND SUBTITLE <b>Optical properties of a bio-inspired gradient refractive index polymer lens</b>				5a. CONTRACT NUMBER	
				5b. GRANT NUMBER	
				5c. PROGRAM ELEMENT NUMBER	
6. AUTHOR(S)				5d. PROJECT NUMBER	
				5e. TASK NUMBER	
				5f. WORK UNIT NUMBER	
7. PERFORMING ORGANIZATION NAME(S) AND ADDRESS(ES) <b>Naval Research Lab, Optical Sciences Division, 4555 Overlook Ave., SW, Washington, DC, 20375</b>				8. PERFORMING ORGANIZATION REPORT NUMBER	
9. SPONSORING/MONITORING AGENCY NAME(S) AND ADDRESS(ES)				10. SPONSOR/MONITOR'S ACRONYM(S)	
				11. SPONSOR/MONITOR'S REPORT NUMBER(S)	
12. DISTRIBUTION/AVAILABILITY STATEMENT <b>Approved for public release; distribution unlimited</b>					
13. SUPPLEMENTARY NOTES					
14. ABSTRACT <b>see report</b>					
15. SUBJECT TERMS					
16. SECURITY CLASSIFICATION OF:			17. LIMITATION OF ABSTRACT	18. NUMBER OF PAGES	19a. NAME OF RESPONSIBLE PERSON
a. REPORT <b>unclassified</b>	b. ABSTRACT <b>unclassified</b>	c. THIS PAGE <b>unclassified</b>			

16. D. T. Moore, "Design of Single Element Gradient-Index Collimator," *J. Opt. Soc. Am.* **67**, 1137-1143 (1977).
  17. J. W. Goodman, *Introduction to Fourier Optics* (McGraw-Hill, San Francisco, CA, 1968).
  18. W. H. Press, S. A. Teukolsky, W. T. Vetterling, and B. P. Flannery, *Numerical Recipes in C: The Art of Scientific Computing* (Cambridge University Press, Cambridge [England]; New York, 1992).
  19. A. Savitzky, and M. J. E. Golay, "Smoothing + Differentiation of Data by Simplified Least Squares Procedures," *Anal. Chem.* **36**, 1627 (1964).
- 

## 1. Introduction

Today's applications are driving a need for smaller, lighter optical devices without any sacrifice in image quality. One way to achieve these goals is to pack more functionality into each lens element. This has renewed the interest in gradient refractive index (GRIN) materials, which are a natural choice for compact optical design.

In nature, where optics are optimized for survival, many species have evolved eyes that use index gradients to enhance focusing power, correct aberrations, and reduce the number of components needed for an effective optical system [1-4]. Human eyes can produce relatively aberration-free images with only two optical components, the cornea and a GRIN crystalline lens. GRIN lenses found in nature typically consist of approximately 22,000 nonplanar layers of proteins with different refractive indices [5]. Systematic variation in protein and water concentration in different layers provides the index gradient [6]. The refractive index range ( $\Delta n$ ) of a human eye lens is about 0.03 [5], and that of some fish eyes can be as high as 0.22 [7].

Inspired by the biological layer motif, we developed a new class of polymer optics with GRIN distributions that can mimic the structures found in biological eyes [8]. The key polymer processing techniques involve the assembly of alternating, nanolayered polymer compounds. These materials permit the fabrication of polymer GRIN lenses with a variety of independently defined index gradients.

The purpose of the present work is to design, fabricate and evaluate properties of an example bio-inspired GRIN lens. The specific lens is relatively fast, at  $f/2.25$ , with an index gradient designed to correct for spherical aberration. Spherical aberration is the primary aberration in fast singlet lenses,  $\sim f/4$  or faster: rays near the edge of the lens are focused in front of the paraxial focal plane. Spherical aberration can be reduced by introducing a shorter optical path near the lens edges via a lower index. In this paper, the techniques for the design and fabrication are described. Then the imaging properties of the bio-inspired polymer GRIN lens are compared with those of a homogeneous, commercial glass lens with a similar  $f/\#$ .

## 2. Lens design and fabrication method

The basic building block of the GRIN lens is a set of transparent nanolayered polymer films, each with a specified refractive index. These are prepared using nanolayer polymer coextrusion technology, *i.e.* forced assembly. This technique produces a film with thousands of alternating layers of two polymers [9] with the individual layer thickness down to less than 10 nm [10, 11]. When the layers are sufficiently thin, the material behaves as an effective medium. It is transparent and the refractive index can be varied smoothly between those of the constituent materials [12] by controlling the relative thickness of the layers.

The lens fabrication procedure is summarized in Fig. 1. First, a set of transparent nanolayered polymer films, each with a specified refractive index, are stacked atop one another. The index profile is determined by the order in which the individual 50  $\mu\text{m}$  films are stacked. Each film is rotated randomly when stacking in order to minimize the birefringence of the final GRIN material. The stack is consolidated at elevated temperatures in a compression molder to give a transparent millimeter-scale-thick polymer sheet. This is the blank for forming the lens. A meniscus lens with both axial and radial gradients is formed by molding them to spherical shapes as shown in Fig. 1. A plano-convex lens is made by cutting

and polishing the concave surface. The final polymer GRIN lens typically contains more than 400,000 nanolayers. By comparison, biological gradient index lenses are typically composed of tens of thousands of protein layers. Attenuated total reflectance Fourier transform infrared spectroscopy (ATR-FTIR) can confirm index distributions in the final lens [8].

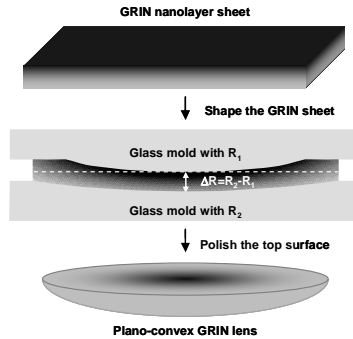


Fig. 1. Schematic for the fabrication of a plano-convex GRIN lens, starting from a heat-pressed GRIN sheet (top). The sheet is molded between concentric glass molds to form a meniscus shape (middle). After release from the molds, the concave surface is polished flat to the white dashed line to form the final lens (bottom).

An  $f/2.25$  lens with an index gradient which corrects for spherical aberration was designed using an optical ray-tracing program, ZEMAX<sup>®</sup> (Zemax Development Corporation, Bellevue, WA). In the fabrication process shown in Fig. 1, the index contours in the lens are concentric spheres which match the curvature of the convex lens surface. Using this constraint, the index distribution was optimized in ZEMAX<sup>®</sup> to minimize spherical aberration and produce the smallest focused spot [13-16]. The optimum index gradient in this case was found to be formed from a lens blank with an index that varies linearly from 1.57 to 1.53 across the blank. The higher index side should be molded to be concave with a 20.67 mm radius of curvature and the low-index surface should be molded convex with a radius of curvature of 23.54 mm. The concave surface is to be polished flat after it is molded to form the desired gradient. Table 1 lists the specifications of the GRIN lens designed for this study.

Table I. Design specifications for the  $f/2.25$  GRIN lens.

Lens diameter	20 mm
Clear aperture	18 mm
Form factor	Plano-convex
Radius of curvature	23.5 mm
Center thickness	2.87 mm
Focal length	41.2 mm
$f/\#$	2.25
Minimum index	1.53
Maximum index	1.57

The polymers used to form the lens were poly(methyl methacrylate) (PMMA) with a refractive index of 1.49 (Plexiglas V920 provided by Atofina Chemicals, Inc), and styrene-acrylonitrile copolymer with 17 wt % acrylonitrile (SAN17) with a refractive index of 1.57 (Lustran provided by Bayer AG). A series of 51 compositions of nanolayered films that differ in refractive index by about 0.0016 was produced by systematically varying the constituent

ratios during coextrusion. Each of these nanolayered films had a thickness of  $\sim 50$   $\mu\text{m}$ . The nanolayered films were extruded with protective peel-off layers of low density polyethylene. The skin layers improved the surface quality of the films and made it easier to exclude contaminants during the stacking process, which took place in a class-10,000 clean room.

The GRIN lens was fabricated to the design specifications starting from a stack of 108 nanolayered films, representing 27 different refractive indices, selected so that the index varied linearly from 1.53 to 1.57. This results in an initial stack  $\sim 5$  mm thick. The target thickness of  $< 3$  mm is attained via the compression and molding steps. The large thickness differential is chosen in order to provide sufficient driving force during fabrication; the fabrications steps are carried out near  $T_g$ , where the material is still relatively stiff. The transmission of these GRIN stacks was measured using Shack-Hartmann techniques. In a typical stack a RMS optical path difference (OPD) of  $\pm 0.12$   $\mu\text{m}$  at 632 nm and a peak-to-valley OPD of 0.64  $\mu\text{m}$  was measured over a 1 cm diameter area. The internal transmission loss was less than  $\sim 2\%$ .

After the sheet was molded, the concave side was diamond turned flat (indicated by the dashed line in Fig. 1.) The convex surface was also diamond turned to correct for any residual deformations. Both lens surfaces were then measured interferometrically. The measured radius of curvature on the convex side was 23.5 mm. The RMS surface deviations were  $\pm 0.2$   $\mu\text{m}$ . The maximum deviation over the planar surface was less than 1.2  $\mu\text{m}$ . The finished lens had a center thickness of  $3.04 \pm 0.01$  mm. Its focal length at 632.8 nm was 41.0 mm. The center thickness was a 6% larger than the target value, but the observed focal length differed from the design by only 0.5%. In our design there is a wide tolerance in the center thickness provided the index values range between the same absolute values.

### 3. GRIN lens optical properties

An index gradient that corrects for spherical aberration should improve both the image quality and ability to collect light. To illustrate this, direct comparisons are provided below to a commercial, biconvex lens made of BK7 glass which has a 38 mm focal length (Newport Optics Inc., Irvine, CA, part # KBX049). Focused light transmitted through pinholes is compared first, followed by a comparison between USAF test chart images. Finally, quantitative modulation transfer function curves are measured and compared to one another. In each comparison, the GRIN lens demonstrates focusing and imaging properties superior to those of the commercial glass lens, which weighed an order of magnitude more than the GRIN lens.

The ability to collect incident light onto a small spot is important for a variety of nonimaging applications of fast lenses. It was measured for both the GRIN lens and the glass lens by focusing a collimated HeNe laser beam (632.8 nm). The HeNe beam had a Gaussian profile and a radius ( $1/e^2$ ) of 8.4 mm. The effective  $f/\#$  of the lenses in the 17 mm mounts was  $f/2.2$  for the homogeneous glass lens and  $f/2.4$  for the GRIN lens. The maximum transmission through a pinhole 50  $\mu\text{m}$  in diameter and one 10  $\mu\text{m}$  in diameter at the focus was measured for the GRIN and the glass lens. For the GRIN lens, a transmission of 66% for the 50  $\mu\text{m}$  and 36% for the 10  $\mu\text{m}$  hole were measured. For the glass lens, the transmissions were 40% and 28%, respectively. The GRIN lens collected 65% more energy through the 50  $\mu\text{m}$  pinhole and 29% more energy through the 10  $\mu\text{m}$  pinhole than the homogeneous lens.

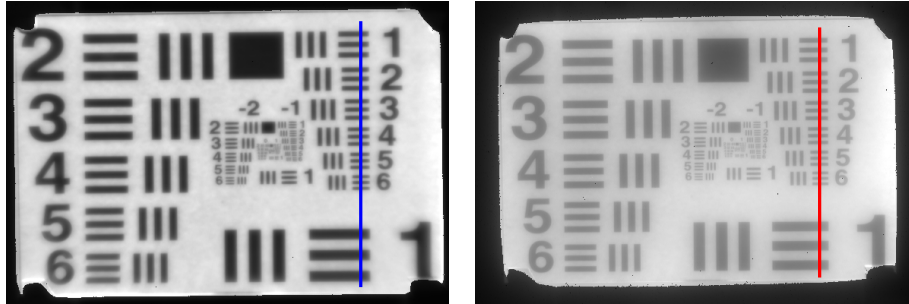


Fig. 2. Images of an Air Force resolution chart taken with the GRIN lens (left) and the glass lens (right). The colored bars represent the data displayed in Fig. 3, below. The slightly different sizes result from the different lens focal lengths: 41.0 mm for the GRIN lens and 38.2 mm for the glass lens.

Shown in Figs. 2 and 3 is a comparison of the image quality obtained through the two lenses, in which it is evident that the contrast of the GRIN image is greatly improved over that of the glass lens. In each case a USAF test chart was placed about 2.5 m from a bare CCD camera. The test charts were laser printed onto standard letter paper and illuminated by a quartz-halogen light source, long-pass filtered at 630 nm. The charts were imaged onto the camera by the singlet lenses. The magnification was 0.017 for the GRIN and 0.016 for the homogeneous glass lens. The top-right element (8 mm/lp on the test chart) is focused to about  $65 \mu\text{m/lp}$  in the image plane. The images were identically processed to correct for single-pixel inhomogeneities and illumination nonuniformity.

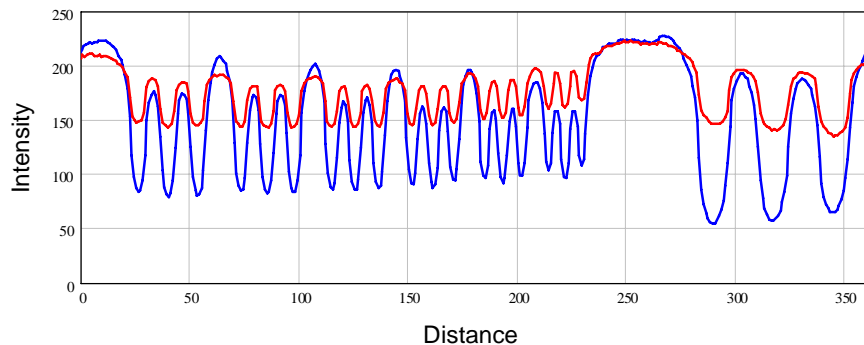


Fig. 3. Plots of the intensity as a function of position for the data from Fig. 3. The blue (red) curve is for the GRIN (glass) lens data. The horizontal scale is in pixels for the GRIN image ( $9.85 \mu\text{m/pxl}$ ). The horizontal axis for the glass data was scaled to match the features in the GRIN image.

In Fig. 2, the center of the field or optical axis is near the horizontal bars of the 2<sup>nd</sup> element of the -2 group. The elements at the bottom corners of the chart are about  $3.5^\circ$  off-axis. At this position in the image plane, field (Petzval) curvature causes the blurring in the GRIN image. Also present in the glass lens image, the field curvature is less apparent because the blurring due to spherical aberration is too large.

Figure 3 shows a plot of the intensity as a function of the distance along the solid lines drawn through the right set of elements in Fig. 2. This provides an illustration of the magnitude of the contrast enhancement in the GRIN image. While rigorous contrast measurements cannot be inferred from 3-bar patterns, and such measurements are further complicated on the USAF test chart by the close proximity of all the other elements, the measured contrast on the left side of Fig. 3 shows about 3 to 3.5 times better contrast in the

GRIN lens. The spacing of the bars in this region corresponds to spatial frequencies near 5 cyc/mm.

Quantitative contrast measurements can be obtained by measuring the modulation transfer function (MTF) of the lenses. This was achieved in two ways. In one case the MTF was measured by resolving a high-contrast edge pattern [17] illuminated with the same filtered broadband source used for the images in Fig. 2. In another, the MTF was calculated from a direct measurement of the on-axis point spread function obtained by focusing a large-area, collimated laser beam onto the CCD camera.

To obtain edge data, large black squares were laser printed onto white paper and illuminated with the same filtered source in the same position as the test charts of Fig. 2. After the raw images were processed in the same way as the images of Fig. 2, edges near the center of the field were superresolved using 30 adjacent rows (or columns) of pixels to generate an edge profile. A Savitsky-Golay smoothing algorithm [18, 19] was used to generate a smoothed line profile and its first derivative, the line spread function (LSF). The MTF calculated from a Fourier transform of the LSF for a horizontal edge is shown as the solid lines in Fig. 4(a). The MTFs in Fig. 4 are corrected for the CCD resolution. The MTF for the GRIN lens is approximately three times (3x) that of the homogeneous glass lens near 5 cyc/mm, and is superior at all spatial frequencies to ~30 cyc/mm.

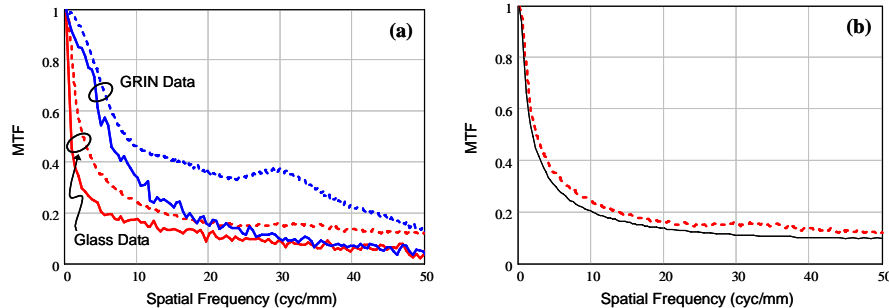


Fig. 4. (a). The modulation transfer function (MTF) measured for the GRIN lens (blue) and the commercial glass lens (red.) The solid lines were extracted from an edge analysis of an imaged chart, while the dashed lines are MTFs extracted from a focused HeNe laser beam. The CCD had a pixel pitch of (8.53 x 9.85)  $\mu\text{m}$ . The units of the horizontal axis correspond to spatial frequency on the camera. (b) Comparison between measured (dashed) and simulated (solid) MTF data for the glass lens. The data curve is identical to the corresponding trace in (a).

The modulation transfer function at a single wavelength (632.8 nm) was also calculated from images of a focused laser beam. As with the pinhole measurements, the incident laser intensity was Gaussian with a  $1/e^2$  intensity radius of 8.4 mm. Since the focal spot intensity varies by several orders of magnitude from the peak to the wings, great care was taken to properly account for noise sources within an image via signal averaging and background subtraction. The resulting MTF curves for each lens are shown as the dashed lines in Fig. 4(a). Comparing the GRIN and homogeneous MTF curves, we see that the MTF of the GRIN lens exceeded that of the glass lens at all spatial frequencies measured. Evidence from other measurements suggest that the peaks near 30 cyc/mm are due to internal processing algorithms in the CCD array for edge enhancement that introduces artifacts at this frequency. While still visible, the peak is largely washed out in the glass lens curve because of the reduced contrast at these spatial frequencies.

To verify the measurement technique, the measured MTF curve for the glass lens was compared to one predicted by standard ray tracing (ZEMAX<sup>®</sup>) software. For a well-characterized lens, such as the homogeneous BK-7 lens, ray tracing gives an accurate

prediction of MTF. Fig. 4(b) shows good agreement between the measured and predicted MTF curves for the glass lens.

#### 4. Discussion

It is clear from Figs. 2-4 that the polymer GRIN lens can focus light tighter, has a better MTF, and produces a higher image quality than the homogeneous glass lens. We have verified that the GRIN profile provides effective aberration correction in an experimental bio-inspired polymer lens.

The differences in the MTFs derived from images of a focused laser beam and those derived from images of objects illuminated with an incandescent light deserve some comment. The differences are highlighted in Fig. 5 where the ratios of the GRIN to the glass MTF curves are plotted for the different illumination conditions. For the MTF derived from imaging high contrast edges, the GRIN lens MTF is three times that of the homogeneous lens near 5 cyc/mm, but the ratio falls with increasing spatial frequency. In this case, the illumination was by broadband visible light. There is no correction for chromatic aberration in either lens. Apparently, spherical aberration dominates at the lower spatial frequencies but chromatic aberration becomes important at higher frequencies. For the MTFs derived from focused laser spot measurements (dashed curve), the GRIN to homogeneous ratio is relatively constant at about two from 5 cyc/mm to 40 cyc/mm. It is reasonable that the maximum value for the ratio is smaller than in the edge imaging experiment. In the Gaussian laser beam, the intensity is greater near the center of the lens. Since the off-axis rays are less important in image formation here, the correction in the GRIN lens provides a smaller advantage. On the other hand, in focusing a laser source, chromatic aberration is unimportant. The advantage of the spherical aberration correction persists to high spatial frequencies.

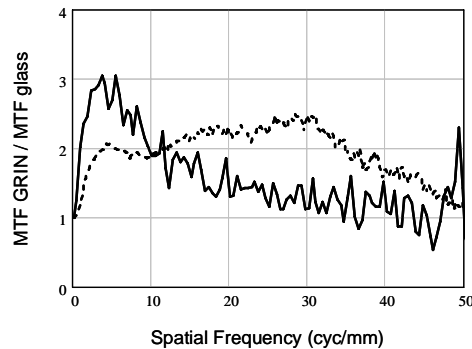


Fig. 5. The ratio of the GRIN to the homogeneous lens MTF. The solid line is the ratio from an edge analysis of a chart illuminated with incandescent light. The dashed line is from an analysis of a focused HeNe laser beam.

The particular homogeneous glass lens was chosen to provide a convenient verifiable reference to evaluate the imaging of the GRIN lens. The absolute magnitude of ratios in Fig. 5 will vary a little for a different reference lens. Ray tracing estimates from ZEMAX<sup>®</sup> predict less than 20% difference in the ratios in Fig. 5 for BK7 lenses with the same focal length but different shape factors. There is little doubt that the polymer GRIN lens described here provides a superior MTF to a comparable homogeneous glass lens.

While the focusing and imaging by the bio-inspired GRIN lens was substantially improved compared to a homogeneous lens, the GRIN lens design used here should theoretically achieve near diffraction-limited performance for normal-incidence laser light. The actual focusing is not diffraction limited. The factors that contribute to the discrepancy in the

current lenses may include the residual phase front errors in the lens blanks, the precision in the surface finish of the lens after the molding and diamond-turning process, or residual birefringence. Many of these effects may be reduced with further processing and fabrication improvements.

One factor that does not appear to affect the lens performance is diffraction of light caused by the variation in refractive index along the planar surface of the lens. Termination of the diamond-turned layers on this surface results in small, step discontinuities of the refractive index. The discontinuous changes in index across the surface result in transmitted wavefronts which are continuous (the thicknesses of the terminated layers smoothly go to zero) but exhibit stepwise discontinuities in their slope. The effect of these discontinuities can be examined in the thin-lens approximation, in which the lens serves as a phase screen with no local ray bending within the element. Within this approximation, the wavefront can be computed and compared to a numerically-smoothed version of the wavefront. Such comparisons reveal that the 'ripple' due to the step discontinuities in the lens has a magnitude  $<0.01$  waves. Using scalar diffraction theory to model otherwise-perfect lenses with radially symmetric phase variations of this magnitude and radial pattern, we find calculated focused spots that differ negligibly from ideal Airy patterns. We conclude that diffractive effects caused by the discrete layers in this lens design are negligible.

## 5. Conclusion

In conclusion, we have shown that the new class of bio-inspired optics introduced in [8] can be represented by optical-quality gradient index lenses which outperform commercial glass singlets in energy concentration and image quality. The impact of the gradient index is clearly evident by inspection of Figs. 2 and 3. Inspired by the structure of eyes in nature, the lenses are comprised of co-extruded polymer nanolayers which provide iso-index thin films which can be stacked in arbitrary order, pressed, molded, and polished into optical-quality lenses. The flexibility of the fabrication method opens the door to a whole new class of gradient index optics.

## Acknowledgments

The authors thank Leonard Buckley, Marie Sandrock, Michael Wiggins and Dean Scribner of the Naval Research Laboratory for many stimulating discussions. Marie and Mike also made important contributions to the initial lens development. G.B. gratefully acknowledges Tom Gutman and Paul W. for their implementation of the Savitsky-Golay smoothing algorithm. We thank Syntec Optics for diamond turning our GRIN lenses. Financial support was provided by the National Science Foundation (NSF), Grant DMR-0349436, and the Defense Advanced Research Projects Agency (DARPA), Grant HR0011-04-C-0043 at Case and the Office of Naval Research and DARPA at the Naval Research Lab.